ELSEVIER

Computer Physics Communications 145 (2002) 141–155

Computer Physics Communications

www.elsevier.com/locate/cpc

Diatomics-in-molecules potentials incorporating *ab initio* data: Application to ionic, Rydberg-excited, and molecule-doped rare gas clusters

F.Y. Naumkin [a], D.J. Wales [b,*]

[a] *Department of Chemistry, University of Toronto, Toronto, ON M5S 3H6, Canada*
[b] *University Chemical Laboratories, Lensfield Road, Cambridge CB2 1EW, UK*

Received 4 May 2001

Abstract

Applications of combined diatomics-in-molecules/*ab initio* approaches to Ne_n^+, Ar_n^*, Ar_nCl_2, and Ar_nNO clusters are discussed. Simple perturbative models within these procedures are suggested to interpret the predicted cluster structures, obtained using a basin-hopping global optimization algorithm. The topological peculiarities of the Ar–NO potential are analyzed in terms of the perturbation of the Ar–N and Ar–O interactions within the complex. The correlation between the solvation of a chromophore species in the cluster and the relative strength of the solvent–solvent and chromophore–solvent interactions is also analyzed.

Keywords: Diatomics-in-molecules; Global optimization

1. Introduction

Rare gas atomic clusters, Rg_n, have been studied for many years as accessible experimental systems with relatively simple isotropic interactions associated with the closed-shell nature of the Rg atoms. The latter simplification also implies that there is usually only one low lying electronic state for such a system.

The properties of ionized clusters, Rg_n^+, are complicated by the open-shell structure, which leads to anisotropic $Rg–Rg^+$ interactions and/or to charge transfer. Both possibilities produce numerous low-lying electronic states associated with different charge distributions and (for Rg heavier than He) different orientations of the half-occupied atomic orbital in Rg^+.

For neutral Rydberg-excited clusters, Rg_n^*, there are also open shell effects and, from an atomistic viewpoint, associated coupling of angular momenta. These effects further extend the variety of possible electronic states in the cluster. For instance, for the lowest-energy excitation of a single Rydberg s-orbital in Rg, there appear singlet and triplet sets of nonrelativistic states, which are further split by spin–orbit coupling.

* Corresponding author.
E-mail addresses: fnaumkin@chem.utoronto.ca (F.Y. Naumkin), wales@cam.ac.uk (D.J. Wales).

0010-4655/02/$ – see front matter
PII: S0010-4655(02)00151-0

For rare gas clusters with embedded molecules or atoms, the electronic structure of the dopand is another factor determining the low-lying states of the system. With a closed-shell molecular or atomic dopand, the situation is similar to that for homoatomic clusters, unless there occurs a significant charge or excitation transfer from the host. With an open-shell dopand, and a ground state Rg_n host, the electronic states of the free dopand may directly correlate with those of the interacting system, except for possible symmetry breaking effects, such as the splitting of a Π state.

Accurate *ab initio* calculations for such weakly bound systems become a serious problem for large n, while the closed-shell nature of rare gas atoms suggests that model potentials may provide a useful alternative. A combination of *ab initio* and empirical potentials therefore appears attractive, using models based on the electronic structure and readily accessible *ab initio* data for small fragments of the system. One such combined approach is based on the diatomics-in-molecules (DIM) method. Here we review recent applications of DIM to various clusters belonging to all the above mentioned categories: pure ionic Ne_n^+, Rydberg-excited Ar_n^*, doped closed-shell Ar_nCl_2 and open-shell Ar_nNO. Some additional data and discussion of the results are also provided.

2. General computational procedure

2.1. DIM potential energy surfaces

The diatomics-in-molecules (DIM) method [1] employs a formally exact separation of the n-atom Hamiltonian

$$\widehat{H} = \sum_{i>j}^{n} \widehat{H}_{ij} - (n-2)\sum_{i}^{n} \widehat{H}_i, \tag{1}$$

into parts corresponding to diatomic (ij) and atomic (i) fragments. The potential energy surface (PES) of the system is therefore decomposed in terms of its fragments by diagonalizing the Hamiltonian matrix **H** constructed in a suitable basis set.

The basis set is constructed from products of atomic wavefunctions of the states reached asymptotically by the total system upon atomization. The diatomic wavefunctions are associated with valence-bond-type linear combinations of atomic functions with the appropriate symmetry properties. For this approach to be useful, the electronic structure of the atoms must be only weakly perturbed within the diatomic fragments and the remainder of the system.

For ionic rare gas clusters, Rg_n^+, the relevant fragments are Rg, Rg^+, Rg_2, Rg_2^+, and for neutral Rydberg-excited clusters we replace $^+$ by *. We consider $3n$ basis functions for the Rg_n^+ or Rg_n^* cluster as follows:

$$\Psi_{i\lambda} = \psi_S(1)\ldots\psi_S(i-1)\psi_{P_\lambda}(i)\psi_S(i+1)\ldots\psi_S(n), \quad i = 1,\ldots,n;\ \lambda = 0,\pm 1,$$

where ψ_S and ψ_{P_λ} represent $Rg(^1S)$ and $Rg^+(p^5\,{}^2P)$ (or $Rg^*(p^5s\,{}^3P)$ for the lowest Rydberg state) wavefunctions, with $\lambda = \pm 1, 0$ the value of the M_L quantum number for the P term. Here we discuss the nonrelativistic case and separate triplet and singlet Rydberg states, which can be considered similarly.

Diatomic wavefunctions are associated with valence-bond-type linear combinations of atomic functions. The Rg_2 ground state $X^1\Sigma_g$ for atoms i and j is associated with all $\Psi_{k\lambda}$ products where $k \neq i, j$. The $Rg_2^{+/*}$ states for atoms i and j are associated with the linear combinations $[\Psi_{i\lambda} \pm \Psi_{j\lambda}]/\sqrt{2}$; these will be $\Sigma_{u,g}$ or $\Pi_{u,g}$ states depending upon λ. Hereafter we drop the multiplicity so that ionic and Rydberg states can be treated simultaneously.

Atomic and diatomic Hamiltonian matrices can now be constructed via

$$\begin{aligned}
&\widehat{H}_i\Psi_{i\lambda} = E(P_\lambda)\Psi_{i\lambda}; \qquad \widehat{H}_i\Psi_{j\lambda} = E(^1S)\Psi_{j\lambda}, \quad j \neq i,\\
&\widehat{H}_{ij}\Psi_{i\lambda} = \tfrac{1}{2}\big[E(\Lambda_u) + E(\Lambda_g)\big]\Psi_{i\lambda} + \tfrac{1}{2}\big[E(\Lambda_u) - E(\Lambda_g)\big]\Psi_{j\lambda},\\
&\widehat{H}_{ij}\Psi_{k\lambda} = E(X)\Psi_{k\lambda}, \quad k \neq i, j,
\end{aligned} \tag{2}$$

with known atomic energies $E(^1S)$, $E(P_\lambda)$, and diatomic potentials $E(X) \equiv E(X^1\Sigma_g)$ and $E(\Lambda_{u,g}) = E(\Sigma_{u,g})$ or $E(\Pi_{u,g})$. Here we use the fact that $\widehat{H}$ can always be partitioned, as in Eq. (1), so that, e.g., $\widehat{H}_i$ is the Hamiltonian of Rg or $Rg^{+/*}$ when the ith atom is in the ground ^1S or ionic/Rydberg-excited P state, respectively. Further transformations of the diatomic matrices are associated with rotation of the quantization axes of separate diatoms to a chosen coordinate system of the cluster, and are determined by the symmetry properties of atomic P-states. If the matrix that specifies rotation of the diatomic axis system to the reference frame is $\mathbf{T}$ then the appropriate diatomic matrix is $\mathbf{H}'_{ij} = \mathbf{T}\mathbf{H}_{ij}\mathbf{T}^{-1}$. Finally, the transformed $\mathbf{H}'_{ij}$ and $\mathbf{H}_i$ matrices are combined in accord with Eq. (1) to produce

$$\mathbf{H} = \sum_{i>j}^{n} \mathbf{H}'_{ij} - (n-2)\sum_{i}^{n} \mathbf{H}_i .$$

We note that this matrix represents the action of $\widehat{H}$ on the column vector of basis functions, $\boldsymbol{\Psi}$, i.e. $\widehat{H}\boldsymbol{\Psi} = \mathbf{H}\boldsymbol{\Psi}$, rather than $\mathbf{H} = \boldsymbol{\Psi}\widehat{H}\boldsymbol{\Psi}^\dagger$. These two possible definitions of $\mathbf{H}$ are only equivalent if the basis is orthonormal. The present approach does not explicitly involve overlap integrals and does not require any orthogonality assumptions for the basis (see Ref. [2] for more discussion).

$\sum_i^n \mathbf{H}_i$ vanishes if the energy origin is chosen as the $(n-1)\mathrm{Rg} + \mathrm{Rg}^{+/*}$ asymptote, since $\sum_i^n \widehat{H}_i\Psi_{j\lambda} = [(n-1)E(^1S) + E(P_\lambda)]\Psi_{j\lambda}$. The diatomic potentials for $\mathbf{H}_{ij}$ can be taken from experiments or high-level *ab initio* calculations, making the DIM procedure semi-empirical or *ab initio*, respectively.

For Rg_n clusters doped with a diatomic molecule, XY, the basic approximation of the traditional DIM approach can be broken if there are strong intramolecular forces perturbing the electronic structure of the atoms X and Y. The Rg–X and Rg–Y interactions are then distorted and cannot be interpreted in terms of isolated RgX and RgY diatomics, unless the basis set is extended to include a sufficient number of their excited states to adequately describe the perturbation. This approach would require accurate XY^*, RgX^* and RgY^* potentials. Alternatively, we can treat XY as another monomer (an effective atom) whose electronic structure is weakly perturbed by the interaction with Rg, which is described by a reliable empirical or *ab initio* PES. For a closed-shell XY molecule, the potential hypersurface of a cluster with n Rg atoms is then approximated as a simple sum of this PES and the Rg_2 interactions, which are usually written as a series starting with two- and three-body terms:

$$V \approx \sum_{i}^{n} V_{\mathrm{Rg}_i\mathrm{XY}} + \sum_{i>j}^{n} V_{\mathrm{Rg}_i\mathrm{Rg}_j} + \sum_{i>j>k}^{n} V_{\mathrm{Rg}_i\mathrm{Rg}_j\mathrm{Rg}_k} + \cdots . \tag{3}$$

For ionic molecules the contribution from the interaction of induced dipoles on Rg atoms may be significant and can be added as a separate term. In particular, for the case of Rg_n^+ clusters considered above, such terms can be added to the diagonal elements of the $\mathbf{H}$ matrix, and then correspond to a specific charge location. For Rg_nXY systems the charge-transfer (or excitation-transfer) between XY and Rg could also be taken into account by considering a $Rg_n^{+/*}$ subsystem, but this approach lies beyond the scope of the present work.

For an open-shell molecule there may be more than one PES associated with the same Rg + XY asymptote, in which case we use a matrix-additive description to generalize Eq. (3) and account for possible mixing of the associated XY states by the interaction with Rg:

$$\mathbf{V} \approx \sum_{i}^{n} \mathbf{V}_{\mathrm{Rg}_i\mathrm{XY}} + \mathbf{I}\left(\sum_{i>j}^{n} V_{\mathrm{Rg}_i\mathrm{Rg}_j} + \sum_{i>j>k}^{n} V_{\mathrm{Rg}_i\mathrm{Rg}_j\mathrm{Rg}_k} + \cdots\right), \tag{4}$$

where $\mathbf{V}$ and $\mathbf{V}_{\mathrm{Rg}_i\mathrm{XY}}$ are matrices in the basis of the relevant XY states and $\mathbf{I}$ is the appropriate identity matrix.

When some RgXY states are sufficiently close in energy, they may be mixed significantly by spin–orbit coupling. The latter contribution can be introduced within the atoms-in-molecules approximation [3] by associating the major contribution with the corresponding spin–orbit Hamiltonian matrix elements for intra-atomic regions unaffected

within the molecule. This matrix is constructed in the specified basis set of XY states and then added to the nonrelativistic potential matrix before diagonalization:

$$\mathbf{V}_{\mathrm{rel}} \approx \mathbf{V} + \mathbf{H}_{\mathrm{SO}}. \tag{5}$$

Mixing between the nonrelativistic states of a molecule can be neglected if the spin–orbit splitting is much smaller than the zeroth order energy separation, as is usually the case for closed-shell molecules in the ground state near equilibrium. This simplification may considerably reduce the dimensionality of $\mathbf{V}_{\mathrm{rel}}$, for example, in ArNO [4], and may produce a scalar potential, as for $ArCl_2$ and ArI_2 [5,6].

2.2. Global optimization

To determine the global potential energy minimum as a function of cluster size we have employed the 'basin-hopping' [7] or Monte Carlo plus minimization [8] approach. The potential energy, E, is transformed to give a new surface:

$$\widetilde{E}(\mathbf{X}) = \min\bigl\{E(\mathbf{X})\bigr\}, \tag{6}$$

where $\mathbf{X}$ is the vector of nuclear coordinates and min signifies that an energy minimization is performed starting from $\mathbf{X}$. An efficient implementation of basin-hopping therefore requires a fast minimization routine, and we currently employ Nocedal's LBFGS algorithm [9] for this purpose.

The transformation defined by Eq. (6) therefore changes the energy at any point $\mathbf{X}$ to the energy of the local minimum obtained after applying some specified minimization algorithm to $E(\mathbf{X})$. The new surface, $\widetilde{E}(\mathbf{X})$, is therefore a set of plateaus, each consisting of those geometries lying in the catchment basin of a given minimum [10]. The most successful applications of global optimization to clusters have all generally employed the above transformation in Eq. (6), either explicitly or implicitly [10]. Hopping between the basins of attraction of different local minima is accelerated because the transition state regions are removed by the $\widetilde{E}$ transformation. All the results described below were obtained by exploring the $\widetilde{E}$ surface using canonical Monte Carlo (MC) sampling at a fixed temperature. At each step all the Cartesian coordinates are perturbed by a random number drawn from the interval $[-1, 1]$ scaled by a maximum step size, which was adjusted dynamically to obtain an acceptance ratio of about a half. Typical maximum step sizes are between 0.3 and 0.4 times a pair equilibrium separation for temperatures a little above the melting point on the transformed landscape.

The convergence criterion for the local energy minimizations need only be tight enough to be sure of distinguishing different structures by their energies. All the lowest minima were optimized to a root-mean-square force of less than 10^{-6} reduced units at the end of each run. In the present work the coordinates were reset to those of the current minimum in the Markov chain at each step, which seems to be the most efficient procedure [11]. The clusters were confined to a spherical container of radius one plus the value required to contain the same volume per atom as the fcc primitive cell. For the present systems the container should have little effect—it basically serves to prevent evaporation.

We used the pair energies, where available, to implement angular displacements of single atoms, enabling them to move around the surface of the cluster more rapidly [7]. If the highest pair energy exceeded a fraction α of the lowest pair energy then the corresponding atom was moved through a random angular displacement, with the other atoms held fixed. The fraction α was adjusted in parallel with the maximum Cartesian coordinate displacement; a typical value was 0.4.

For each cluster size five runs of 5000 or 10,000 MC steps were performed from random starting geometries. These short runs are generally sufficient for the relatively small clusters considered in the present work; all five runs usually produced the same lowest minimum. As a check we also included runs of 200 steps starting from the global minima obtained for the clusters containing one atom more and one atom less. Starting from the cluster containing $n-1$ atoms we only allowed angular moves of the nth atom during the first 100 steps. Starting from

the global minimum at $n+1$ the atom with the highest pair energy was removed and 200 unrestricted Monte Carlo moves on the transformed landscape were then allowed.

For clusters containing dopands such as NO and Cl_2 the dopand coordinates were held fixed and only the Rg atoms were moved. We did not find it necessary to optimize the temperature of the MC basin-hopping runs very carefully for the present systems. Typically we used temperatures corresponding to about a pair well depth for the rare gas atoms, with maximum atomic displacements of order 1 Å. Our results can be downloaded from the Cambridge Cluster Database [12].

The basin-hopping approach appears to work well for two reasons. Firstly, the elementary moves between local minima correspond to relatively large distances in configuration space. The system can pass between local minima at any point on the catchment basin boundary, and atoms can even pass through each other. However, the thermodynamic properties of the transformed surface are also helpful in locating the global minimum for multi-funnel landscapes [13]. The occupation probability of the funnel corresponding to the global minimum on the transformed landscape has been found to remain significant at temperatures where the inter-funnel free energy barriers are still relatively small. This feature of the transformation helps to overcome one of the central problems of global optimization, namely that the free energy minimum changes at a temperature where the free energy barriers are too large to overcome on the time scale of the calculation.

3. Results and discussion

3.1. *Ionic and Rydberg systems:* Ne_n^+ *and* Ar_n^*

The above DIM model for $Rg_n^{+/*}$ was employed [2,14] to investigate the structures of Ne_n^+ and Ar_n^* clusters for $3 \leqslant n \leqslant 25$. High-level *ab initio* data [2,15] for Ne_2^+ (coupled-cluster level) and Ar_2^* (multireference CI level) potentials, together with accurate empirical ground state Ne_2 and Ar_2 curves [16,17], were used as input.

Fig. 1 shows the PES of the Ne_3^+ ground $^2\Sigma^+$ and Ar_3^* lowest Rydberg $^3\Sigma^+$ states for linear ($C_{\infty v}$) geometries. Both systems exhibit symmetric ($D_{\infty h}$) equilibrium configurations; the well for Ne_3^+ is flatter and for Ar_3^* the minimum is separated from the $Ar + Ar_2^*$ asymptote by a small potential barrier. These Σ_u^+ configurations have the charge/excitation distributed over all three atoms, but concentrated mainly on the central atom, especially for Ar_3^*.

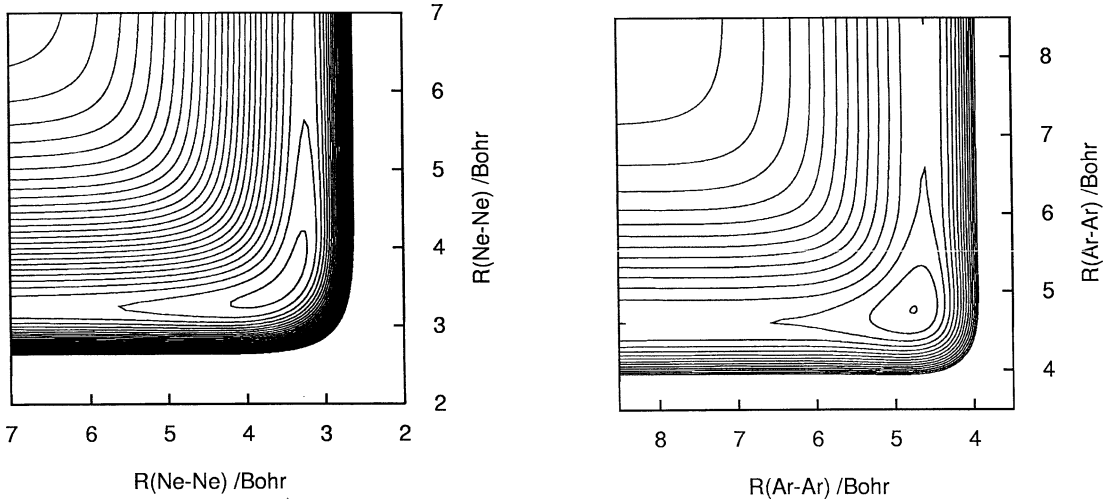

Fig. 1. DIM potential energy surfaces for Ne_3^+ (left) and Ar_3^* (right) in the linear ($C_{\infty v}$) geometry. The contour step is 2 mhartree.

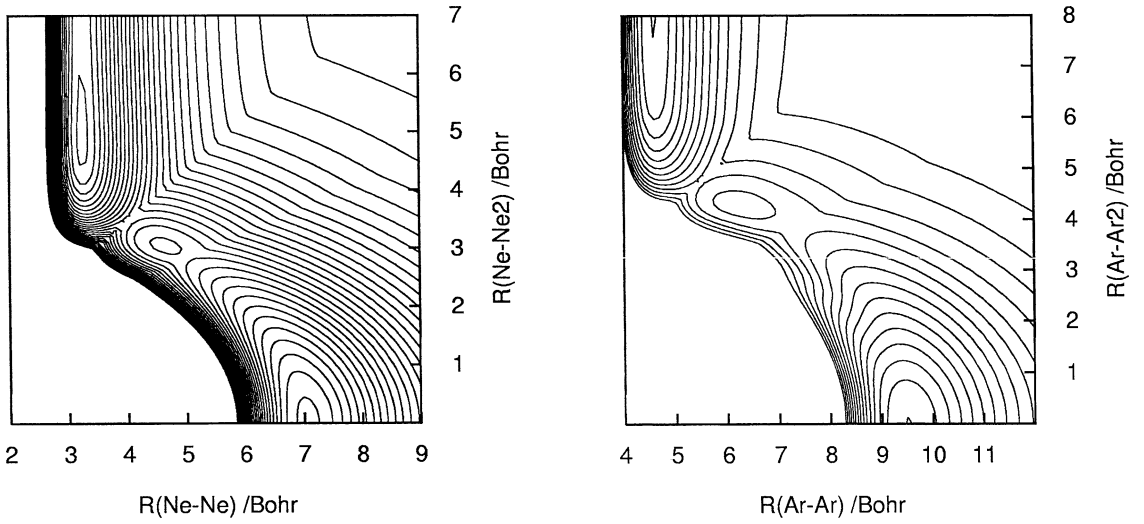

Fig. 2. DIM potential energy surfaces for Ne_3^+ (left) and Ar_3^* (right) in the T-shaped (C_{2v}) geometry. The contour step is 2 mhartree.

DIM results for Ne_3^+ have been shown [18] to reproduce *ab initio* results of accuracy equivalent to that employed for the diatomic curves, but do not support the other local minimum corresponding to a linear asymmetric configuration Ne–Ne_2^+, found in *ab initio* calculations [19–21].

The ionic system has also a somewhat shallower local minimum for the T-shaped (C_{2v}) geometry (Fig. 2), corresponding to the polarization interaction of Ne with almost unperturbed Ne_2^+, and separated from the global minimum for the linear geometry by a significant barrier. A similar, though slightly lower barrier, exists for the Rydberg system, but no noticeable binding occurs for Ar in the T-shaped geometry because of the electrical neutrality of Ar_2^*. For each system the minor higher-energy minimum near the barrier top is due to intersection with a low-lying excited state of different symmetry. No other low-energy minima have been found for Rg–$Rg_2^{+/*}$ in any geometry.

To interpret the structure of larger clusters obtained with the DIM potential, we consider the interaction of a single atom with the triatomic core. We first consider a simplistic model, assuming this interaction to be weak enough not to perturb the charge/excitation distribution. At equilibrium, Ne_3^+ is then approximately represented as Ne–Ne^+–Ne with probability $q_0 \approx 50\%$ and Ne^+–Ne–Ne or Ne–Ne–Ne^+ with probability $q_1 \approx 25\%$ each. The corresponding values for Ar_3^* are 80 and 10% [2,14]. The Rg–$Rg_3^{+/*}$ potential can then be written as

$$V \approx q_0 V_{010} + q_1 (V_{100} + V_{001}), \tag{7}$$

where V_{010}, V_{100}, and V_{001} are the Rg–(Rg–$Rg^{+/*}$–Rg), Rg–($Rg^{+/*}$–Rg–Rg), and Rg–(Rg–Rg–$Rg^{+/*}$) potentials, respectively. This expression coincides with the result of first-order perturbation theory applied within the DIM framework. The potential can be split into diatomic components, such as

$$V_{010} = V_{\mathrm{Rg-Rg}} + V_{\mathrm{Rg-Rg^{+/*}}} + V_{\mathrm{Rg-Rg}}, \tag{8}$$

with each component evaluated at the interatomic distance corresponding to the configuration of interest. We can use accurate empirical Rg_2 potentials for $V_{\mathrm{Rg-Rg}}$ and take into account the anisotropy of $V_{\mathrm{Rg-Rg^{+/*}}}$ via a proper valence-bond combination of the $Rg_2^{+/*}$ potentials:

$$V_{\mathrm{Rg-Rg^{+/*}}} = \tfrac{1}{2}(V_{\Sigma_u} + V_{\Sigma_g}) \cos^2\theta + \tfrac{1}{2}(V_{\Pi_u} + V_{\Pi_g}) \sin^2\theta, \tag{9}$$

where θ is the polar angle of Rg relative to the position of $Rg^{+/*}$.

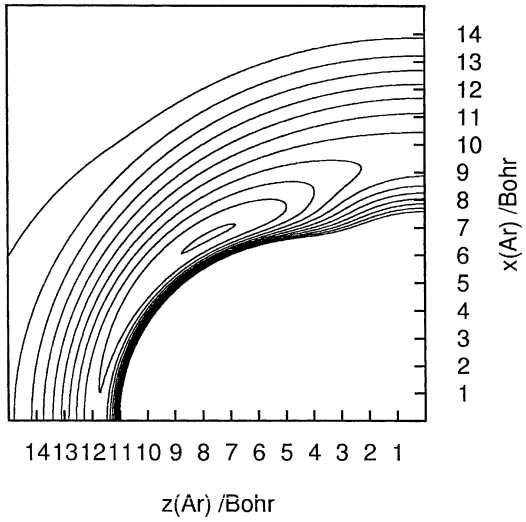

Fig. 3. Model potential energy surfaces for the interaction of Ar with Ar_3^* fixed at its equilibrium geometry and positioned at the origin along the z-axis. x and z are the coordinates of Ar relative to the centre of Ar_3^*. The contour step is 0.05 mhartree.

For the Ar–Ar_3^* interaction, this simple model predicts saddle points at both the linear and T-shaped configurations, and a very shallow minimum for a bent configuration, with the fourth Ar at about 45° from the central atom of the core (Fig. 3). Full DIM calculations [2] confirm this result and predict Ar_3^* to exist as an almost unperturbed core in larger clusters, with more ground state Ar atoms filling the shallow well near one end of the core and forming equilibrium neutral Ar_{n-2} structures that include the nearest core atom. We therefore predict that 'magic number' clusters, which are particularly stable relative to neighboring sizes, should occur for Ar_n^* at $n = 9$, 15, 21 and 25, because the corresponding magic numbers for Ar_{n-2} occur at 7, 13, 19 and 23 (Fig. 4). Full DIM results confirm that the Ar_3^* core is only weakly perturbed as n increases. The core thus remains attached to the cluster surface, at least in the size range $n \leqslant 25$, unlike Ar_n^+ clusters where the Ar_3^+ core is surrounded by neutral atoms [22–24].

However, the perturbative model fails for the Ne–Ne_3^+ interaction, predicting a saddle point for the linear configuration and a wide well for the T-shaped configuration. Complete DIM calculations, allowing for arbitrary charge redistribution, predict instead formation of a symmetric ($D_{\infty h}$) Ne_4^+ structure with most charge ($2q_0 \approx 92\%$) on two closely spaced central atoms. This result is different from the relatively stable triatomic core in Ar_n^+ clusters [22–24], and is a consequence of the topology of the Ne_3^+ PES, which is very flat along the antisymmetric stretch coordinate (Fig. 1), so that the interaction with an additional Ne atom is a strong perturbation. The $D_e(Ne_n^+ \rightarrow Ne_{n-1}^+ + Ne)$ dissociation energies [2] support this conclusion, since the dissociation energy for Ne_4^+ is 35% of that for Ne_3^+, compared to 13% for Ar_4^* versus Ar_3^*, which explains the accuracy of the perturbative treatment for the latter Rydberg system.

We can modify the perturbation model to allow for a tetra-atomic core by adding an extra term:

$$V \approx q_0(V_{0100} + V_{0010}) + q_1(V_{1000} + V_{0001}). \tag{10}$$

This potential predicts a saddle point for the linear configuration of Ne_4^+ interacting with a single Ne atom, and a deeper and wider well near to the T-shaped configuration, with shoulders at about 3 bohr from the equilibrium geometry (Fig. 5). This result is consistent with the structures obtained for larger clusters [2], where additional Ne atoms form a 'belt' in the central plane of the Ne_4^+ core until we reach $n = 9$ (a magic number), after which two such belts appear at the shoulders of the potential (Fig. 6). Full DIM results suggest that the Ne_4^+ core is only weakly perturbed up to $n = 14$ (another magic number). When more neutral atoms are added, the core becomes an

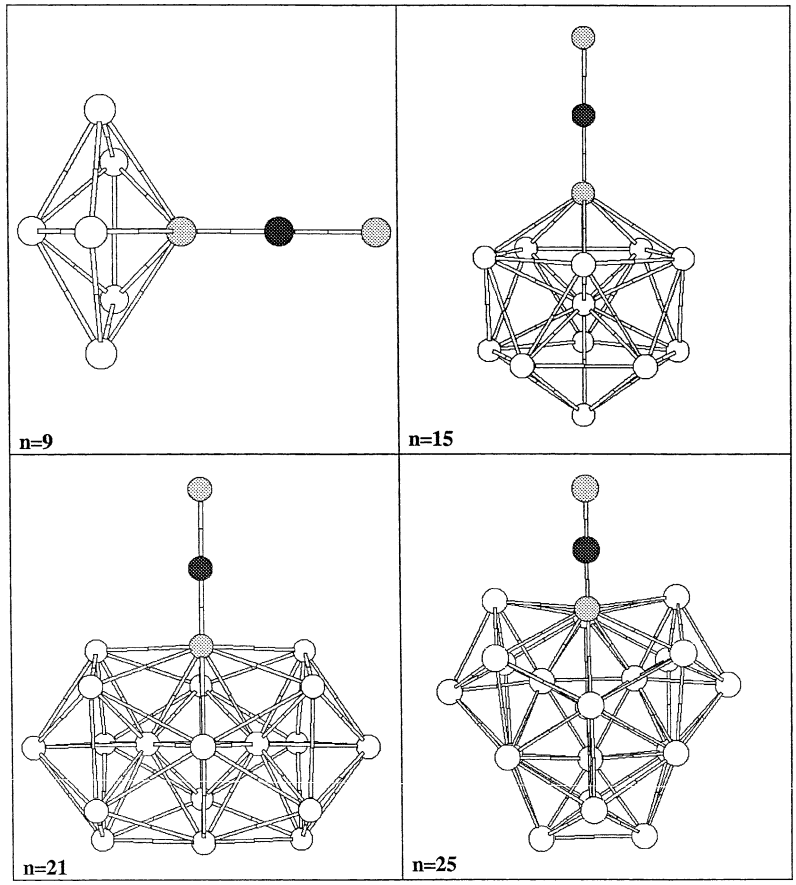

Fig. 4. Selected global minima Ar_n^* clusters: $n = 9$, 15, 21, 25. The shading indicates the excitation distribution.

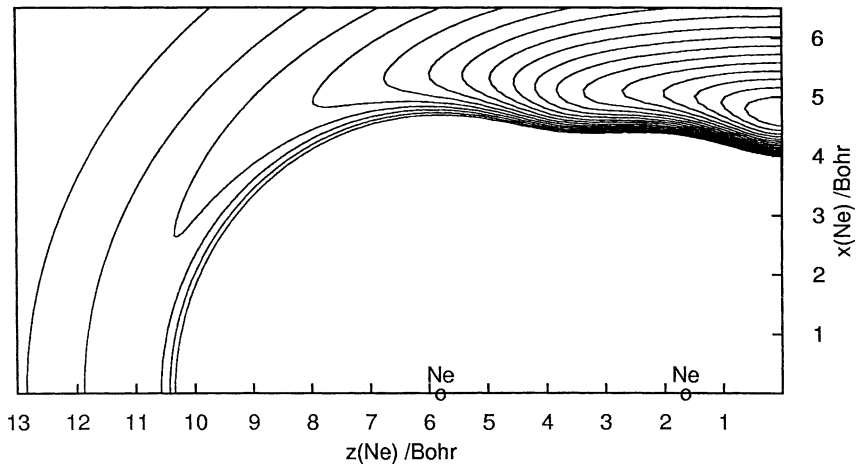

Fig. 5. Model potential energy surface for the interaction of Ne with Ne_4^+ fixed at its equilibrium geometry and positioned at the origin along the z-axis. x and z are the coordinates of Ne relative to the centre of Ne_4^+. The contour step is 0.1 mhartree.

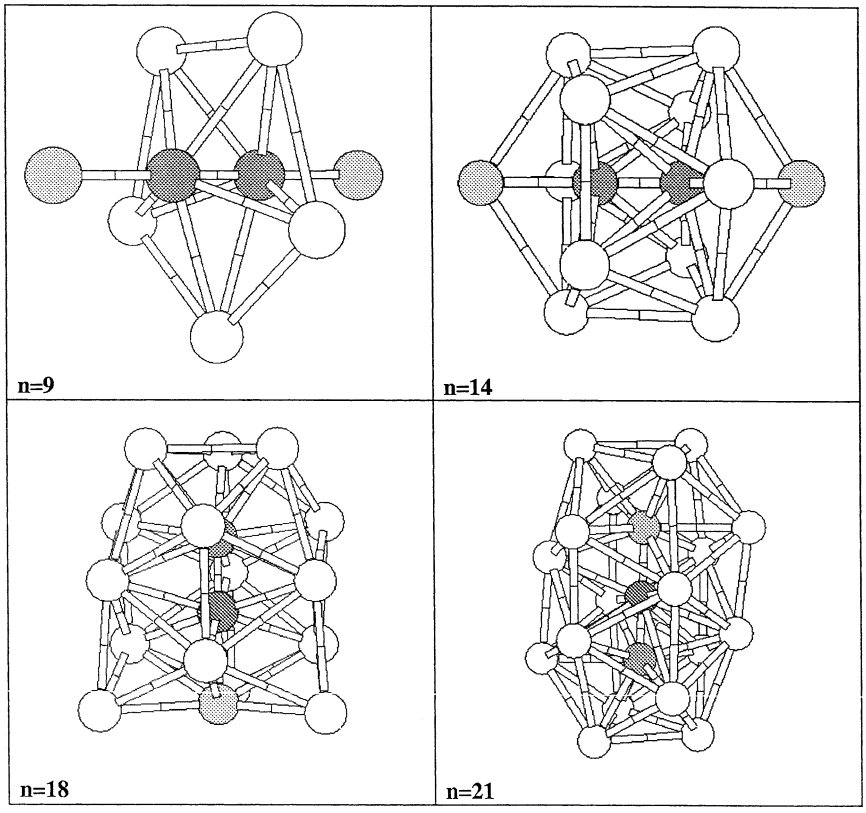

Fig. 6. Selected global minima Ne_n^+ clusters: $n = 9$, 14, 18, 21. The shading indicates the charge distribution.

asymmetric triatomic with two atoms bearing most of the charge, and is gradually solvated as n increases further. The diatom bearing most of the charge is solvated at $n = 18$ and the whole triatomic core is solvated at $n = 21$, both these sizes exhibiting 3-fold symmetry and corresponding to magic numbers.

We can attempt to predict whether or not the core will be solvated by comparing the Rg–core and Rg–Rg interactions. Since a solvated core is surrounded by atoms, the isotropic component of the corresponding potential, representing an angular average, is likely to be the most important term. In the case of Ar_n^* the situation is straightforward, and we consider the angular average of the $Ar–Ar_3^*$ potential. In the case of Ne_n^+, the core changes with cluster size, but always includes a diatom carrying $\geqslant$92% of the charge plus one or two almost neutral atoms. It seems therefore reasonable to assume that the $Ne–Ne_2^+$ interaction is mainly responsible for the core solvation.

The isotropic component of the $Ne–Ne_2^+$ potential provides stronger binding than the Ne–Ne potential, as expected from the extra electrostatic terms. The averaged $Ar–Ar_3^*$ interaction turns out to be somewhat less attractive than the Ar–Ar potential. These results are in good agreement with the observed degree of solvation of the respective cores in the ionic and Rydberg clusters, found by the full DIM approach.

3.2. *Closed-shell and open-shell dopands:* Ar_nCl_2 *and* Ar_nNO

For the interaction of the closed-shell ground state Cl_2 molecule with Ar atoms, the simple pairwise-additive potential (3) can be used. The contribution of 3-body interactions was investigated [25] and found to be unimportant, at least in the range $2 < n < 25$. A high-level *ab initio* $Ar–Cl_2$ PES [5], scaled to accurately reproduce the experimental bond energy and microwave spectrum, was employed.

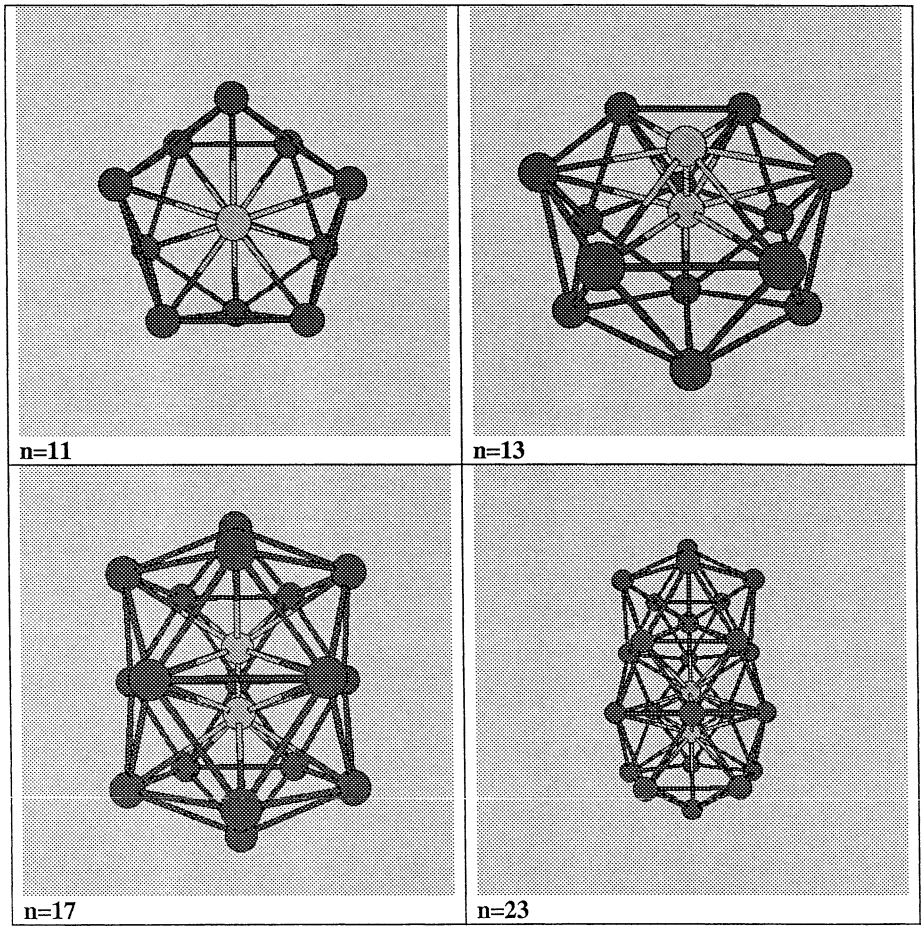

Fig. 7. Selected global minima Ar_nCl_2 clusters: $n = 11$, 13, 17, 23.

The Ar–Cl_2 PES exhibits two local minima of similar depth for the linear (L) and T-shaped configurations, due to the anisotropy of the Ar–Cl interaction and because the ArCl($^2\Sigma^+$) potential exhibits a well about twice as deep as that for ArCl($^2\Pi$). This situation favors Ar_nCl_2 structures with Ar atoms occupying positions near the T-shaped configuration, for small n. As n increases the presence of the L-well starts to be felt, and we find that in the lowest energy structures the Cl_2 core turns so that one end points towards the Ar_n substructure and sinks into it (Fig. 7). One end of the Cl_2 molecule is still in the surface at $n = 11$, giving a C_{5v} global minimum with an Ar atom lying along the core axis and two five-atom belts around the middle. The C_{6v} $n = 13$ global minimum is similar, with two six-atom belts. Both these clusters are particularly stable relative to neighboring sizes, with large contributions to the binding energy from the argon subsystem in $n = 13$ and the Ar–Cl_2 interactions in $n = 11$ [4]. As n increases further the core becomes completely surrounded by Ar atoms in the predicted global minima. Further local stability maxima appear at $n = 15$ and $n = 17$, the latter cluster exhibiting a D_{5h} double icosahedron structure, with the Cl_2 atoms occupying the central sites (Fig. 7). The next 'magic' size appears not at $n = 20$, which has three six-atom belts, but instead at $n = 23$, where the double icosahedron motif is extended by another axial atom and a fourth five-atom belt. Both $n = 17$ and 23 are particularly stable due to favorable Ar–Cl_2 interactions.

The observed solvation of Cl_2 by Ar_n is consistent with the angularly averaged Ar–Cl_2 potential, which exhibits a deeper minimum than exists for Ar_2.

The nonrelativistic Ar–NO($^2\Pi$) interaction is asymptotically doubly degenerate with respect to the states of A' and A'' symmetry, which correspond to the half-occupied π-orbital of NO parallel and perpendicular to the Ar–N–O plane, respectively. In the van der Waals region these two states are split and two distinct PES's result due to the open-shell character of NO. The main features of these surfaces can be interpreted using an anisotropic atom–atom model. The relevant ArN($^4\Sigma^-$) potential remains isotropic in Ar–NO if we assume that the N atom is unperturbed. The Ar–O interaction, however, is clearly anisotropic due to the difference between the $X\,^3\Sigma^-$ and $^3\Pi$ Ar–O potentials. By relating the electronic configuration of NO to the occupation of orbitals in N and O, the Ar–NO PES can be expressed approximately in terms of the corresponding ArN and ArO potentials:

$$\begin{aligned} &V_{\mathrm{Ar\text{–}NO}(A',A'')} \approx V_{\mathrm{ArN}} + V_{\mathrm{ArO}(A',A'')},\\ &V_{\mathrm{ArO}(A')} = V_{\mathrm{ArO}(\Pi)}\cos^2\theta_{\mathrm{O}} + V_{\mathrm{ArO}(\Sigma)}\sin^2\theta_{\mathrm{O}}, \qquad V_{\mathrm{ArO}(A'')} = V_{\mathrm{ArO}(\Pi)}, \end{aligned} \tag{11}$$

where θ_{O} is the polar angle of Ar relative to O with NO fixed at its equilibrium geometry.

PES's corresponding to Eq. (11) and employing *ab initio* Ar–N and Ar–O potentials are shown in Fig. 8. They are degenerate for the linear geometry, and have deep minima near the T-shaped configuration, slightly

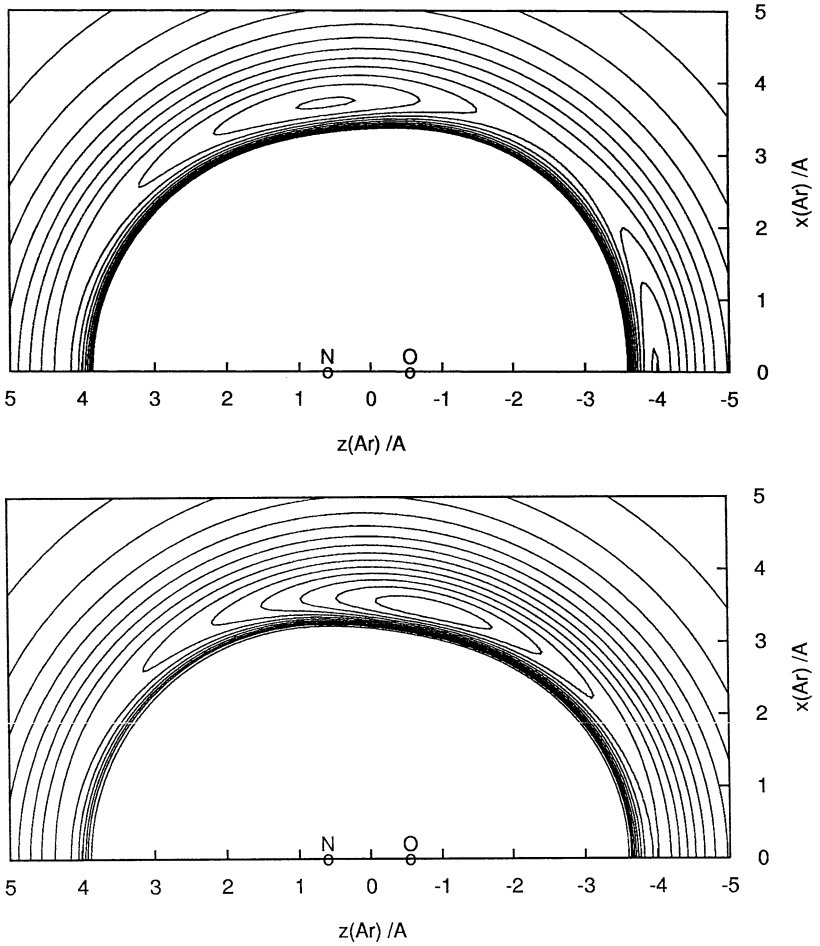

Fig. 8. Model A' (upper) and A'' (lower) potential energy surfaces for the interaction of Ar with NO($X^2\Pi$) fixed at its equilibrium geometry and positioned at the origin along the z-axis. x and z are the coordinates of Ar relative to the centre of NO. The contour step is 1 meV.

shifted towards the N or O end for the A' and A'' states, respectively. The A' PES shows another minimum for the linear Ar–O–N configuration due to the anisotropy of the Ar–O potential, but this feature becomes a saddle point on the A'' PES, for which the latter diatomic potential is isotropic. For both states the model defined by Eq. (11) predicts a saddle point for the linear Ar–N–O configuration as a consequence of the isotropic Ar–N potential.

Full *ab initio* calculations, at the same level of theory as for the diatomic potential curves, are in good agreement with most of the above features [4]. However, they also predict a shallow well for the linear Ar–N–O configuration on the A' PES and the deep minima move a little towards opposite ends of the NO molecule. At this level of theory both surfaces are somewhat more attractive than the model of Eq. (11), and the deepest minima are more stable with respect to bending. These differences can be attributed to the perturbation of the Ar–N and Ar–O potentials due to the electron density redistribution associated with the formation of a strong N–O bond, which is not accounted for by the simple model. In particular, both the displacement of the deepest well in the A'' state towards the N end of NO, and the appearance of the nearby shallow minimum in the A' state, are consistent with a shift of electron density from N to O, in accord with the dipole moment of NO.

The above two states represent a natural basis for relativistic calculations, since the nonrelativistic ground state of NO is well separated (by several eV) from the first excited state around the equilibrium distance of interest. Relatively weak spin–orbit coupling effects can therefore significantly mix the A' and A'' states. The spin–orbit Hamiltonian matrix in such a basis set can be represented using an atoms-in-molecules formalism [4], using a 2×2 matrix and a single parameter Δ, chosen to reproduce the experimental splitting of the lowest $\Omega = 1/2$ and 3/2 states of NO. The resulting relativistic Ar–NO surfaces are then

$$V_{\mathrm{Ar\text{–}NO}(1/2,3/2)} \approx \tfrac{1}{2}\big[V_{\mathrm{Ar\text{–}NO}(A')} + V_{\mathrm{Ar\text{–}NO}(A'')} \mp \sqrt{(V_{\mathrm{Ar\text{–}NO}(A')} - V_{\mathrm{Ar\text{–}NO}(A'')})^2 + \Delta^2}\,\big]. \tag{12}$$

These surfaces have different energies for any configuration and the topologies are mixtures of the nonrelativistic results. The deepest minimum shifts closer to the T-shaped configuration for both states, and is only slightly displaced towards the O end of NO for the $\Omega = 1/2$ state and the N end for the $3/2$ state (Fig. 9). The well for the linear Ar–O–N configuration for the A' state flattens due to the saddle point that appears there in the A'' state. Similar behaviour was obtained using *ab initio* surfaces [4].

For Ar_nNO clusters, the A' and A'' states associated with each Ar are mixed according to the orientation of the half-occupied NO π-orbital with respect to the particular Ar–N–O plane. This mixing can be expressed in terms of 2×2 matrices $\mathbf{V}_{\mathrm{Ar\text{–}NO}}$ in the basis of two orthogonal π-orbitals of NO [4], which are then added together to produce the total matrix $\mathbf{V}$ for the cluster as in Eq. (4). Diagonalization of this matrix, with the spin–orbit matrix added for the relativistic case, yields analytic expressions for the PES of Ar_nNO, which can be written as [4]

$$V_{\mathrm{Ar}_n\text{–}\mathrm{NO}(1/2,3/2)} \approx \sum_{i>j}^{n} V_{ij} + \frac{1}{2}\Bigg[\sum_{i}^{n}(V_i' + V_i'') \mp \sqrt{\sum_{i}^{n}(V_i' - V_i'')^2 + 2\sum_{i>j}^{n}(V_i' - V_i'')(V_j' - V_j'')\cos 2(\phi_i - \phi_j) + \Delta^2}\Bigg], \tag{13}$$

where $V_{ij} = V_{\mathrm{Ar}_i\mathrm{Ar}_j}$, $V_i' = V_{\mathrm{Ar}_i\text{–}\mathrm{NO}(A')}$, $V_i'' = V_{\mathrm{Ar}_i\text{–}\mathrm{NO}(A'')}$ and ϕ is the torsional angle of the Ar atom. Even in the absence of spin–orbit coupling ($\Delta = 0$), these surfaces differ from the pairwise-additive result for a closed-shell molecular dopand unless either all the Ar atoms and NO are in the same plane ($\phi_i = \phi_j$ for all i and j), or the A' and A'' states are essentially degenerate ($V_i' \approx V_i''$), when Eq. (13) reduces to Eq. (3). For the relativistic case the two PES's remain split for any configuration.

For each Ar–NO pair the spin–orbit coupling parameter $\Delta \approx 120\ \mathrm{cm}^{-1}$ is considerably larger than the energy difference between the two nonrelativistic states, which are therefore strongly mixed. This mixing results in similar

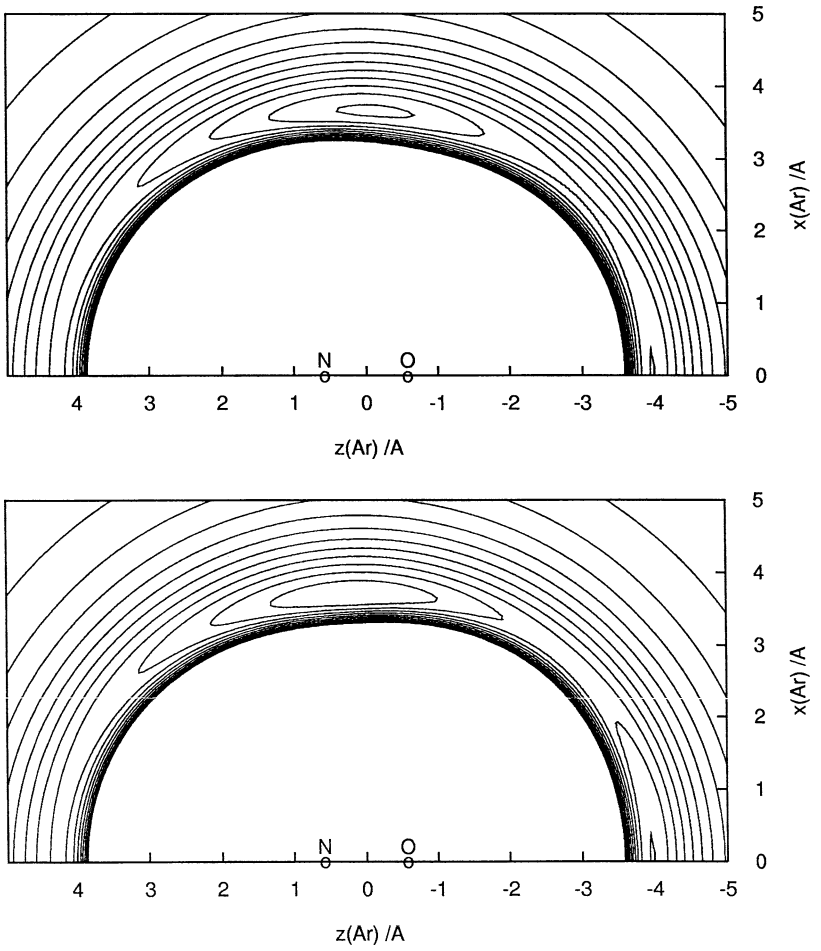

Fig. 9. Model Ar–NO(X 1/2) (upper) and Ar–NO(3/2) (lower) relativistic potential energy surfaces. The coordinates and contours are the same as in Fig. 8.

surfaces for $\Omega = 1/2$ and $3/2$, which are close to the average of the A' and A'' surfaces, split by about Δ everywhere [Eq. (12)]. If we assume that this approximation holds for more than one argon atom, then Eq. (13) reduces to a pairwise-additive potential and the relativistic Ar–NO surfaces represent the interaction of each Ar with NO within the cluster.

The approximately T-shaped equilibrium configuration of Ar–NO is consistent with the Ar_nNO global minima [4], in which both atoms of NO usually lie in the surface of the Ar_n subsystem, or are partly submerged in it with the closest Ar atoms forming T-shaped units. The isotropic component of the Ar–NO interaction is slightly less attractive than the Ar_2 potential, which is consistent with a surface location for NO in the clusters and with the predicted magic sizes at $n = 6$, 12, 18, 22, corresponding to those for Ar_m with $m = n + 1$ (Fig. 10). These sizes are found to be particularly stable with respect to dissociation channels associated with detachment of Ar or NO, and are structurally almost identical to the global minima predicted for pure argon clusters when NO is replaced by another argon. The structures and magic numbers are the same for both relativistic states due to the similarity of their PES's.

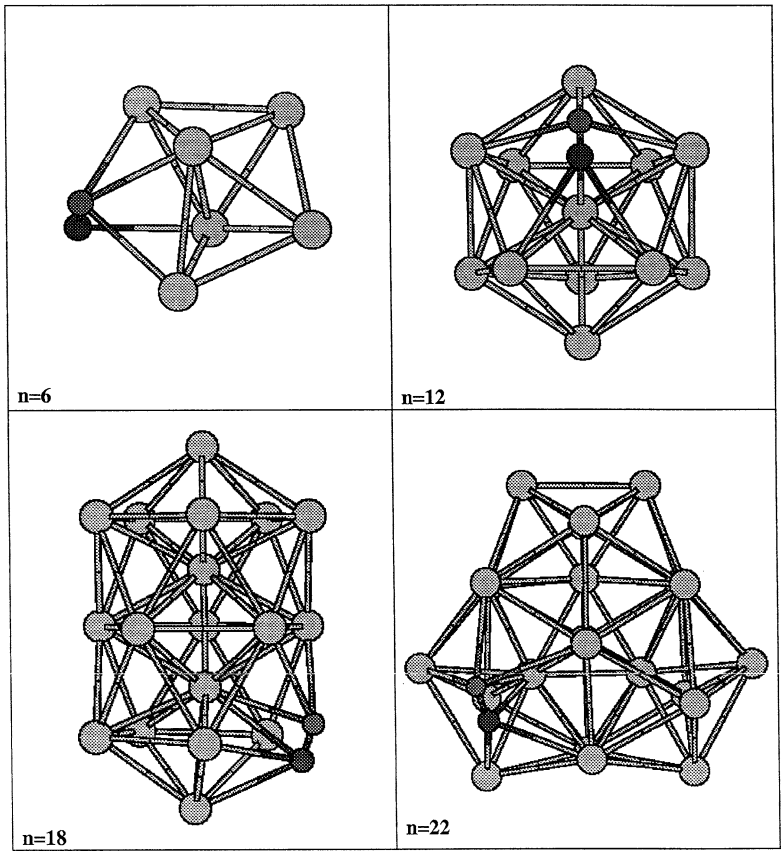

Fig. 10. Selected global minima $Ar_n NO$ clusters: $n = 6$, 12, 18, 22.

4. Conclusions

Application of DIM procedures involving *ab initio* atom–atom and atom–molecule potentials as input have been illustrated for rare gas clusters that are ionic, Rydberg-excited, or doped with a closed- or open-shell molecule. The total potential energy surfaces are obtained from DIM models at different levels of theory, ranging from the simplest pairwise-additive assumption to diagonalization of appropriate Hamiltonian matrices. In the latter case, simple perturbative approximations have been employed to interpret the predicted cluster global minima.

While in Ne_n^+ the ionic core is surrounded by neutral atoms, the Ar_3^* core of Ar_n^* is attached to the surface of the remaining Ar cluster via a shared atom. This result can be viewed as a surface exciton described by electronic structure calculations. As a consequence of this structure, it is energetically favorable for the Ar_3^* core to detach from the rest of the cluster as a whole rather than by releasing the protruding diatom [14]. Ionization of the Rydberg-excited state in a cluster is likely to cause a considerable structural change associated with the charge sinking into the bulk of cluster.

For molecule-doped clusters, the molecular dopand XY can be treated as an effective atom whose interaction with Rg atoms is represented by an Rg–XY PES. Comparison of simple atom–atom models for such surfaces with full *ab initio* calculations allows us to predict and interpret the main topological features and to analyse how the surfaces are affected by perturbation of the X, Y atoms within the molecule. In particular, for ArNO the associated distortions of the Ar–N and Ar–O potentials lead to the intersection of the A' and A'' nonrelativistic surfaces [4], which is removed by spin–orbit coupling.

In general, the structures of pure Rg_n clusters are significantly perturbed by solvation of either a charge, as in Ne_n^+, or a molecule, as in Ar_nCl_2. In cases where solvation is unfavorable, as for the Rydberg excitation in Ar_n^* or the molecular dopand in Ar_nNO, the host structure is generally preserved by isolating the excitation in the surface (for Ar_n^*) or by incorporating the dopand as another pseudo-atomic unit (for Ar_nNO). Whether or not solvation occurs appears to be predictable by considering the relative binding between Rg atoms and between Rg and the dopand or the core that carries the charge or excitation.

The predicted cluster global minima have been used to predict the Ne_n^+ and Ar_n^* photoabsorption spectra, Ne_n ionization, Ar_n Rydberg excitation, Ar_n^* emission, and $Ar_nNO(1/2 \rightarrow 3/2)$ spectra [2,4,14].

Acknowledgements

This paper was prepared while FN held a visiting assistant professorship in the group of Professor J.C. Polanyi.

References

[1] F.O. Ellison, J. Amer. Chem. Soc. 85 (1963) 3540.
[2] F.Y. Naumkin, D.J. Wales, Mol. Phys. 93 (1998) 633.
[3] J.S. Cohen, B.J. Schneider, J. Chem. Phys. 61 (1974) 3230.
[4] F.Y. Naumkin, D.J. Wales, Mol. Phys. 98 (2000) 219.
[5] F.Y. Naumkin, F.R.W. McCourt, J. Chem. Phys. 107 (1997) 5702.
[6] F.Y. Naumkin, Chem. Phys. 226 (1998) 319.
[7] D.J. Wales, J.P.K. Doye, J. Phys. Chem. A 101 (1997) 5111.
[8] Z. Li, H.A. Scheraga, Proc. Natl. Acad. Sci. USA 84 (1987) 6611.
[9] D. Liu, J. Nocedal, Math. Programming B 45 (1989) 503.
[10] D.J. Wales, H.A. Scheraga, Science 285 (1999) 1368.
[11] R.P. White, H.R. Mayne, Chem. Phys. Lett. 289 (1998) 463.
[12] D.J. Wales, J.P.K. Doye, A. Dullweber, F.Y. Naumkin, M.P. Hodges, The Cambridge Cluster Database, http://www-wales.ch.cam.ac.uk, 2001.
[13] J.P.K. Doye, D.J. Wales, Phys. Rev. Lett. 80 (1998) 1357.
[14] F.Y. Naumkin, D.J. Wales, Mol. Phys. 96 (1999) 1295.
[15] F. Spiegelmann, F.X. Gadea, J. de Phys. 45 (1984) 1003.
[16] R.A. Aziz, M.J. Slaman, Chem. Phys. 130 (1989) 187.
[17] R.A. Aziz, J. Chem. Phys. 99 (1993) 4518.
[18] F.Y. Naumkin, P.J. Knowles, J.N. Murrell, Chem. Phys. 193 (1995) 27.
[19] H. Hogreve, Chem. Phys. Lett. 215 (1993) 72.
[20] A.-M. Sapse, K. Shukla, J. Mol. Struct. 307 (1994) 23.
[21] J. Urban, P. Mach, J. Masik, I. Hubac, V. Staemmler, Chem. Phys. 255 (2000) 15.
[22] P.J. Kuntz, J. Valldorf, Z. Phys. D 8 (1988) 195.
[23] T. Ikegami, T. Kondow, S. Iwata, J. Chem. Phys. 98 (1993) 3038.
[24] N.L. Doltsinis, P.J. Knowles, F.Y. Naumkin, Mol. Phys. 96 (1999) 749.
[25] F.Y. Naumkin, D.J. Wales, Chem. Phys. Lett. 290 (1998) 164.